HMT production and sublimation during thermal process of cometary organic analogs. Implications for its detection with the ROSETTA instruments

Giacomo Briani *, Nicolas Fray *, Hervé Cottin, Yves Benilan, Marie-Claire Gazeau, Sebastien Perrier

Laboratoire Interuniversitaire des Systèmes Atmosphériques (LISA), UMR 7583 du CNRS, Université Paris Est – Créteil (UPEC), Université Paris Diderot (UPD), 61 Avenue du Général de Gaulle, 94010 Créteil, France

ABSTRACT

One important component of refractory organic residues synthesized from interstellar/cometary ice analogues is hexamethylenetetramine (HMT, $C_6H_{12}N_4$). However, HMT has never been observed in any astrophysical or planetary environment so far. We investigated thermal evolution of HMT above ambient temperature. The synthesis of the organic residue (ice deposition, photolysis and warming) as well as its heating to temperatures higher than 300 K are performed by means of the same experimental apparatus. The later also allows *in situ* continuous monitoring of both the solid organic residue (by FTIR spectrometry) and of the gas species (by mass spectrometry).

Two different ice mixtures, composed of $H_2O:CH_3OH:NH_3 = 10:1:1$ and $H_2O:CH_3OH:NH_3:CO_2 = 10:1:1:2$, were deposited and simultaneously photolyzed at 29 K. Warming these photolyzed ices up to 300 K allows the production of refractory organic residues. At 300 K the organic residues clearly show the presence of HMT, but also some difference, in particular in their oxygenated components. Different evolutions of the organic residues are observed for temperatures >300 K.

We characterized the organic residue thermal evolution for temperatures up to 500 K. We observed that HMT is still produced at temperatures higher than 300 K. Production of solid HMT and sublimation are simultaneous. HMT observed in the solid phase could be only a minor fraction of the total HMT production, the major fraction being sublimated. The kinetics of the HMT thermal evolution strongly depends on the organic residue composition at 300 K and seems to depend on the exact nature of the oxygenated fraction of the organic residue. The maximum temperature at which solid HMT is observed is 450 K. As HMT forms only for temperatures greater than 280 K in laboratory conditions, it implies that the detection of solid HMT in extraterrestrial samples will provide a strong indication of their thermal history. Consequently, the search for HMT in both solid cometary grains and gaseous phases in the coma of Comet 67P/Churyumov–Gerasimenko will have to be performed by the Rosetta space mission, in particular with the COSIMA and ROSINA instruments.

1. Introduction

Comets are considered as the most primitive objects in the Solar System. Indeed dark, low altered asteroids and comets exhibit a continuum of compositions and structures (Gounelle, 2011). However, comets were formed in the outer, cold regions of the Solar System (beyond the "snow line", i.e. where temperature is low enough for water ice to condense) and experienced less thermal alteration than asteroids which formed in the inner, warmer regions (Brownlee, 2003). Hence, comets are expected to contain the most pristine information about the physico-chemical conditions which were prevailing in the solar nebula at the time of the planetesimal formation. Moreover, numerous comets fell into the primitive Earth and brought surface water and organic material which could have enabled the emergence of life (Chyba et al., 1990). The chemical characterization of cometary nuclei is of prime interest for the understanding of planets formation and emergence of life on Earth.

Cometary nuclei are composed of icy mixtures of volatile compounds, minerals and refractory organic matter. Even if only water ice has been directly detected thanks to its 1.5 and 2 µm absorption bands at the surface of Comet 9P/Tempel nucleus (Sunshine et al., 2006), the nature and the abundances of the other volatile molecules (mostly organic) present in cometary nuclei in the solid state are relatively well known from remote sensing observations

of the gaseous phase of the coma at different wavelengths (Bock-elée-Morvan et al., 2004). The nature of minerals can also be probed by thermal emission in the infrared (Hanner and Bradley, 2004). In particular, the presence of Mg-rich crystalline silicates has been clearly revealed in cometary grains of C/1995 O1 (Hale–Bopp) (Crovisier et al., 1997, 2000). Moreover, the analysis of 81P/Wild (Wild 2) comet grains, returned by the Stardust mission in 2006, revealed numerous details concerning the mineralogy of the comets (Zolensky et al., 2006; Flynn, 2008). However, unlike volatile molecules and minerals, the physico-chemical nature of refractory organic matter remains very elusive.

The *in situ* measurements of cometary grains by mass spectrometers (PIA on board of Giotto (Kissel et al., 1986a), PUMA-1 and 2 on board of Vega 1 and 2, respectively (Kissel et al., 1986b) and CIDA on board of Stardust (Kissel et al., 2004), have shown that organic matter is also present in the form of a complex refractory component. As some of these grains seem to be mainly composed of solid organic matter made of carbon, hydrogen, oxygen and nitrogen atoms, they have been called "CHON grains" (Fomenkova, 1999). These *in situ* observations have also shown that "CHON" grains could be different one from each other, suggesting that cometary organic matter is heterogeneous at a very small scale in cometary nuclei (Fomenkova et al., 1994). Nevertheless, very few information was collected about the chemical nature of this refractory carbonaceous matter. Although the analysis of the grains returned by the Stardust probe has revealed the presence of various chemical functions by infrared spectroscopy and C-XANES (Sandford et al., 2006), the contamination of the aerogel (Sandford et al., 2010) makes the final interpretation of the data extremely difficult (Muñoz Caro et al., 2006, 2008) and only glycine has been firmly identified in 81P/Wild (Wild 2) grains so far (Elsila et al., 2009). Chondritic-porous interplanetary dust particles (CP-IDPs) and ultracarbonaceous Antarctic micrometeorites (UCAMMs) represent unaltered samples of mostly probable cometary origin (Bradley, 2003; Duprat et al., 2010). They show abundant organic matter which experienced a very low degree of metamorphism (Dobrică et al., 2011; Davidson et al., 2012), characterized by different textures and morphologies (Matrajt et al., 2012), containing aliphatic hydrocarbons (Flynn et al., 2000), polycyclic aromatic hydocarbons (Clemett et al., 1993; Dobrică et al., 2011) and showing elevated H and N isotopic anomalies (Floss et al., 2006; Duprat et al., 2010). In addition to observations and analysis of samples having extraterrestrial origin, experiments can be conducted in the laboratory to mimic the synthesis of cometary refractory organic matter from ice mixtures submitted to energy deposition: UV, particles, thermal cycles (Bernstein et al., 1995; Cottin et al., 1999; Colangeli et al., 2004).

The temperatures experienced by the refractory organic content of comets have strong implications on its final molecular structure and composition. During the last decade, it has become more and more apparent that the thermal history of the cometary matter is extremely complex and that materials from various origins in the solar nebula are mixed. On the one hand, water ice has been detected at the surface of 9P/Tempel 1 (Sunshine et al., 2006) as well as in grains ejected in the cometary atmosphere (Lellouch et al., 1998). Furthermore, cometary nuclei contain very volatile compounds such as CO and CH_4 which have been detected in gas phase in the coma (Bockelée-Morvan et al., 2004). These observations show that part of the cometary nuclei has experienced only very low temperatures most of the time since its formation. On the other hand, some crystalline silicates have been detected in cometary grains (Crovisier et al., 1997; Hanner and Bradley, 2004; Keller et al., 2006). All the mechanisms proposed to explain the presence of Mg-rich crystalline silicates in comets require very high temperatures, of about 1000 K (Wooden et al., 2007). Consequently, silicate crystallization should have occurred in the solar nebula

before their incorporation in cometary nuclei. Then, cometary refractory organic compounds are certainly a mixture of primitive and thermally evolved molecules. This could explain the heterogeneity of the chemical properties of the CHON grains measured in the environment of 1P/Halley (Fomenkova et al., 1994).

Once in the coma, the small cometary grains can reach temperatures higher than the blackbody temperature. For example, grains having a radius lower than 0.1 μm can reach 500 K at 1 AU (Kolokolova et al., 2004). Laboratory simulations showed that, at these temperatures, refractory organic compounds, such as polyoxymethylene, undergo thermal decomposition (Fray et al., 2004) leading to the production of gaseous molecules. This could be responsible for the observation of distributed sources in cometary environment (Cottin and Fray, 2008) as well as the decrease of the proportion of particles containing organic material with increasing nucleus distance (Fomenkova et al., 1994).

Studying the thermal evolution of organic residue from low (∼10 K) to high (∼600 K) temperature is necessary to: (i) constrain the thermal alteration that refractory organic matter could undergo in the solar nebula before their incorporation into cometary nuclei, and (ii) explain the processes that take place in the coma. In this paper, we present a new experimental setup designed to study the thermal evolution up to 600 K of organic residues produced from the VUV photolysis of ice mixture at low temperature. So far, the thermal evolution of icy mixtures and organic residues, also called "yellow stuff", have mainly been analyzed between 10 and 300 K (Greenberg, 1982; Bernstein et al., 1995; Muñoz Caro and Schutte, 2003; Bossa et al., 2009; Meinert et al., 2012). Infrared spectra of organic residue annealed to temperatures up to 500 K were previously reported by Muñoz Caro et al. (2006). Hexamethylenetetramine ($C_6H_{12}N_4$, hereafter HMT) is one of the major components of refractory organic residues synthesized from interstellar/cometary ice analogues (Bernstein et al., 1995; Muñoz Caro and Schutte, 2003). However, HMT has never been observed in any astrophysical or planetary environment. In this paper, we report the thermal evolution of the organic residue during heating between 300 and 600 K, and we discuss in particular the formation and disappearance of HMT.

In Section 2, we will present the experimental setup which has been specifically developed for the study of the thermal evolution of organic residues at high temperature ($T > 300$ K). Such organic residues are synthesized from ice mixture photolysis at low temperature ($T \sim 20$ K). We will present the experimental protocol in Section 3, our results in Section 4 and we will discuss their astrophysical significance in Section 5.

2. Experimental setup

The OREGOC experimental setup (OREGOC stands for *ORigine et Evolution des Glaces et des composés Organiques Cométaires*, which means Origin and Evolution of Cometary Ices and Organics) is composed of a high vacuum chamber in which the temperature of a sample holder can be controlled between 20 and 800 K. Gas mixture is condensed on the sample holder at low temperature and simultaneously photolyzed using VUV lamp. The evolution of the solid sample is characterized by Fourier transform infrared spectrometry (FTIR) and the gas phase produced during sample heating is analyzed by mass spectrometry. This device has already been used to study the thermal degradation of polyoxymethylene (Le Roy et al., 2012) as well as the chemical mechanisms of HMT formation during the heating of photolyzed ice mixture (Vinogradoff et al., 2013).

2.1. Vacuum chamber

The high vacuum stainless steel chamber is kept to a pressure of ∼10^{-8} mbar at room temperature by means of a turbo pump

(Varian turbo-V 301) backed up by a primary pump (Varian SH110). The vacuum chamber has 8 external ports (see Fig. 1). The sample holder is located at the center of the high vacuum chamber. This sample holder is connected to a closed-cycle helium cryostat via a resistive heater and a thermal protection switch which allow controlling its temperature from 10 to 800 K. The configuration (see Fig. 1) is such that the sample holder: (1) is at the level of the gas injection tubes; (2) is oriented at 45° with respect to the axial direction of the VUV photon flux; (3) crosses the beam of the IR spectrometer at an angle of 45°; (4) is in front of the mass spectrometer. Such a configuration allows performing (i) the gas injection to form the initial ice film, (ii) the photolysis of the ice by VUV photons, (iii) the monitoring of the solid sample by FTIR spectrometry and (iv) the analysis of the gases emitted from the solid sample by mass spectrometry simultaneously without moving the sample holder.

2.2. Cryostat and sample holder

The closed-cycle helium cryostat (DE-204 AF T, Advanced Research Systems, Inc.) can cool the sample down to 20 K. The temperature of the second stage of the cryostat is measured thanks to a silicon diode. Two thermocouples (one type E and one Au Fe–Cr) and a Platinum resistance are fixed between the resistive heater and the sample holder. These four detectors, as well as the resistive heater, are connected to a temperature controller (LakeShore 340) which regulates the temperature by means of a proportional–integral-derivative (PID) feedback mechanism. The sample temperature can be controlled from 20 to 800 K. A thermal temperature switch made of sapphire is located between the cryostat and the electric resistance. The sapphire window is thermally conductive at low temperature and is thermally insulative at high temperature. This allows performing ice deposition at very low temperature ($\sim$20 K) and subsequently warming up the sample to 800 K, whereas the temperature of the cryostat second stage is kept lower than 300 K. The sample holder is a copper support covered by Ag in which an IR transparent CsI window is mounted using an indium seal to ensure good thermal conductivity. The diameter of the CsI windows is 10 mm.

2.3. Preparation of gas mixture

The gas mixtures prepared for our experiments contained in various proportion: H_2O (liquid, triply distilled); CH_3OH (liquid,

Fig. 1. Schematic representation of a horizontal section of the OREGOC experimental setup.

Sigma–Aldrich 99.9%); CO (gas, Air Liquid 99.997 %); CO_2 (gas, Air Liquid 99.998%) and NH_3 (gas, Air Liquid 99.999%). The gas mixtures are prepared thanks to a gas line composed of two separate parts to prevent reactions at room temperature: one for NH_3 and one for the other gases. The gas line can be evacuated down to a pressure of $\sim 10^{-7}$ mbar by a turbo molecular pump (Pfeiffer TMH 071) backed by a diaphragm pump (Pfeiffer vacuum MVP 015–2). The pressure in the gas line is monitored by two Baratron pressure gauges (MKS 627 B), one with a full scale range of 1.33 mbar and the second one with a full scale range of 1333 mbar. The gas mixture is prepared by filling the volume of a bulb with the different gases, except NH_3, to obtain the desired gas partial pressures. The flow toward the vacuum chamber of the H_2O:CH_3-OH:CO_2:CO mixture is regulated using a micrometric valve, whereas the injection of NH_3 in the vacuum chamber is regulated by a mass flow controller (MFC 1179B, MKS), which assures a constant gas flow between 0.2 and 10 sccm (sccm = standard cubic centimeters per minute).

Several calibration experiments were carried out in order to determine the correct conditions that provide the desired ice growth rate and NH_3 molecular ratio in the ice mixtures. Different upstream pressures (always lower than 20 mbar to prevent condensation in the gas line) were tested in the injection line, as well as different apertures of the micrometric valve for the injection of the H_2O:CH_3OH:CO_2:CO mixture and different regulations of the MFC for the injection of NH_3. As the MFC requires an upstream pressure of about 1 bar, to achieve the desired NH_3 flow, NH_3 has been diluted in He, which is not incorporated in the ice given the temperature of the sample holder.

2.4. VUV lamp

The VUV photons used for the ice photolysis are produced by a microwave-powered plasma lamp in which an H_2—He mixture (98% He, 2% H_2) flows. This mixture allows maximizing the intensity of the H Lyman α (121.6 nm) emission (Davis and Braun, 1968) whereas the VUV emission spectra show also a large band centered at about 160 nm. Previous works indicate that the photon flux emitted with this type of VUV lamp is about 10^{15} photons s^{-1} (Warneck, 1962; Davis and Braun, 1968). We calibrated the VUV lamp photon irradiance impinging our solid sample by performing actinometry experiment on a thick CO_2 ice film. Even if the ice film was thick, the combination band at 3600 cm^{-1} is not saturated and thanks to the infrared integrated cross sections measured by (Gerakines et al., 1995), we can estimate a CO_2 column density of 5.5×10^{18} molecules cm^{-2}. Then, considering the CO_2 ice VUV cross section measured by (Mason et al., 2006), we calculated that 98% of the H Lyman α (121.6 nm) photons are absorbed and that only 10% of the 160 nm photons are absorbed. During the photolysis, we followed the appearance of CO by infrared spectroscopy. Using the CO band strength published in Gerakines et al. (1995), we measured an appearance rate of 1.6×10^{13} molecules cm^{-2} s^{-1}. As all the photons are not absorbed by the CO_2 ice film and as the photolysis products, CO and O atoms, can recombine into CO_2, we consider that the VUV photon irradiance received by our samples is at least 1.6×10^{13} photons cm^{-2} s^{-1}.

2.5. FTIR and mass spectrometry

The evolution of the solid sample (from the initial ice to the final organic residue) is monitored by transmission infrared spectroscopy (Bruker – Vertex 70 FTIR spectrometer). We collected FTIR spectra in the wavenumber range 400–5000 cm^{-1} at a resolution of 1 cm^{-1}. Each spectrum corresponds to a mean of 256 scans giving time steps of $\sim$390 s. The IR signal is collected by an external
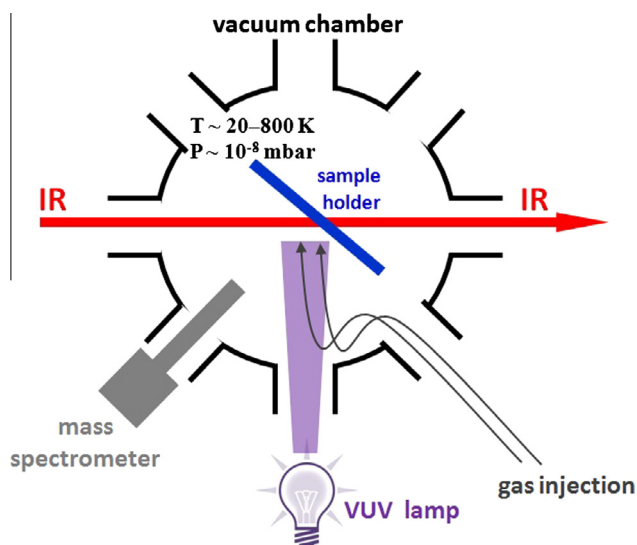
detector (MCT D316/B). The FTIR spectrometer and the external pathway to the detector are kept under dried atmosphere. Gaseous species emitted from the solid sample are characterized by means of a quadrupole mass spectrometer (QMG 220, Prisma Plus, Pfeiffer Vacuum). Mass spectra are continuously acquired in the m/z range 0–200, with a mass resolution Δ (m/z) ~ 1. Each mass spectrum corresponds to a time interval of $\sim$125 s.

3. Experimental protocol

3.1. Ice deposition and photolysis

For each experiment a new CsI window is used for sample deposition in order to avoid contamination from previous experiments. First we inject all the gases at the desired flow rate when the sample holder has reached a constant temperature of 29 K. A visual inspection of the first four FTIR spectra allows verifying that the initial ice composition is correct (Fig. 2). Then, we switch on the VUV lamp. The ice deposition and photolysis are performed simultaneously at constant temperature during more than 15 h (Fig. 3). The exact deposition and photolysis durations are indicated in Table 1.

The initial ice composition was chosen on the basis of the determination of molecular abundances in ices of dense molecular clouds (Gibb et al., 2004; Dartois, 2005) and comets (Bockelée-Morvan et al., 2004). It was close to the one used in some previous laboratory works dealing with organic residues synthesis from ice photolysis (Bernstein et al., 1995; Muñoz Caro and Schutte, 2003).

The standard experiment with initial ice composition $H_2O:CH_3OH:NH_3:CO_2 = 10:1:1:0$ was repeated three times to check the reproducibility of our results (Table 1: experiments #1 to #3, hereafter Exp#1, Exp#2 and Exp#3, respectively). For one experiment (experiment #4, hereafter Exp#4), we added CO_2 to study the influence of this molecule on the nature and thermal evolution of the final organic residue. For this experiment, CO was present in the initial gas mixture ($H_2O:CH_3OH:NH_3:CO_2:CO = 10:1:1:2:1$). However, as the gas mixture is injected at 30 K, only a minor fraction of CO condensed in the ice (this explains the very small CO feature in Fig. 2). Two blank experiments were performed (Table 1): one with the same ice deposition than the standard experiment but without VUV photolysis (experiment #5) and one without any ice deposition (experiment #6).
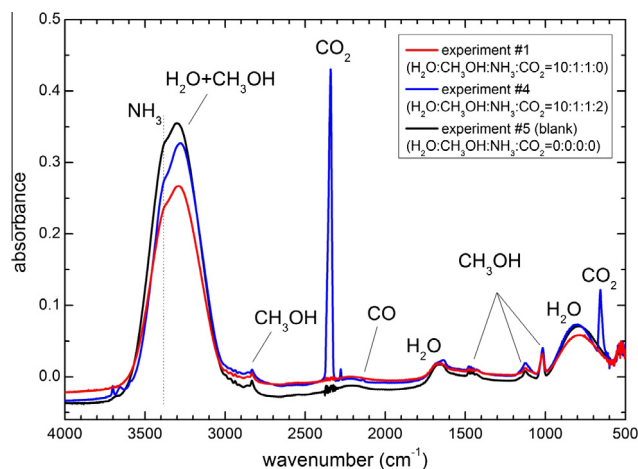

Fig. 2. FTIR spectra of the deposited ice measured about 1000 s after the beginning of the gas injection and before the beginning of VUV photolysis. All the injected gases are present in the ice, as attested by their principal IR peaks. Details about the experiments can be found in Table 1.
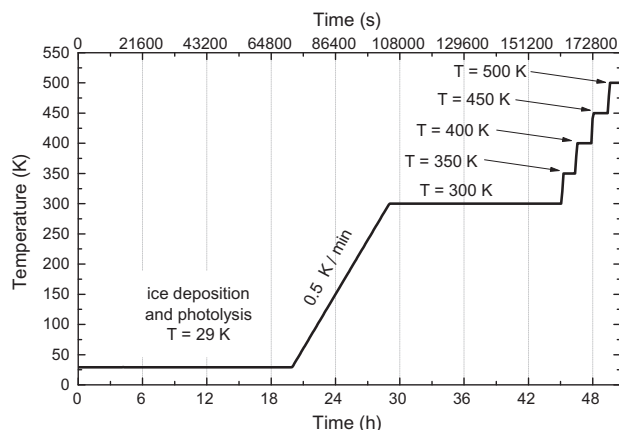

Fig. 3. The temperature evolution in the OREGOC experiments reported in this work.

3.2. Temperature evolution

In all experiments, we increased the sample temperature only after stopping ice deposition and VUV photolysis. The sample temperature was raised up to 300 K at a constant rate of 0.5 K/min (Fig. 3). Once the sample had reached 300 K, it was maintained at this constant temperature for $\sim$16 h. We did not observe significant variations of neither FTIR nor mass spectral features during this period. Then, we increased the temperature by successive steps of 50 K each (Fig. 3) to study the thermal evolution of the organic residue at $T > 300$ K. For all the experiments, the time interval spent by the sample at a given temperature is of the order of 80 min for 350 K $< T <$ 500 K. The maximum difference among these time intervals in different experiments is 3 min.

4. Results

4.1. Blank experiments

FTIR spectra of blank experiments (Exp#5 and Exp#6; see Table 1) do not show any significant feature between 400 and 5000 cm^{-1} at any temperature. The noise in absorbance is always lower than 3×10^{-3}. Therefore we consider that contamination is negligible in all FTIR spectra.

Mass spectra collected during the blank experiments confirm that no significant contaminants are present since no peak due to organic molecules was observed. Nevertheless, as the total pressure is about 10^{-8} mbar, we observed, in these mass spectra, peaks due to residual atmospheric gases, such as N_2 and O_2. Blank experiments revealed, however, that the 50 K temperature steps cause a sudden and global increase in the intensity of mass spectra. In order to take into account this behavior when analyzing mass spectra of the gaseous phase emitted from the organic residue during the heating, we always compared mass spectra to those measured in the blank experiments.

4.2. The organic residue at 300 K

As we are interested in the high temperature ($T > 300$ K) evolution of HMT, we consider the organic residue at the end of the 300 K constant temperature step as the starting point for the analysis of our results. A detailed description of the chemical synthesis at $T < 300$ K of the organic residue is reported in Vinogradoff et al. (2013). In Fig. 4, we present the FTIR spectra of the organic residues synthesized in our experiments: Exp#1 and Exp#4. The FTIR peak assignments are reported in Table 2.

Table 1
Summary of the experiments.

Experiment	Ice composition[a] $H_2O:CH_3OH:NH_3:CO_2$	Ice deposition temperature (K)	Photolysis time	Gas injection speed[b] (molecules s^{-1})	Dose[c] (photons/ molecules)
Exp#1	10: 1: 1: 0	29	15 h 40 min	$(1.1 \pm 0.2) \times 10^{15}$	>0.01
Exp#2	10: 1: 1: 0	29	15 h 33 min	$(1.1 \pm 0.2) \times 10^{15}$	>0.01
Exp#3	10: 1: 1: 0	29	15 h 42 min	$(1.1 \pm 0.2) \times 10^{15}$	>0.01
Exp#4	10: 1: 1: 2	29	15 h 42 min	$(1.1 \pm 0.2) \times 10^{15}$	>0.01
Exp#5	10: 1: 1: 0	29	0	$(1.1 \pm 0.2) \times 10^{15}$	0
Exp#6[d]	0: 0: 0: 0	29	0	0	0

[a] Estimated on the basis of gas partial pressures in the gas injection column and ice growth rates in calibration experiments.
[b] Estimated on the basis of calibration experiments.
[c] Estimated using a photon flux on the sample equal to 10^{13} photons/s, as determined by CO_2 actinometry experiments (see text).
[d] Experiment #6 is a blank. We went through the complete protocol shown in Fig. 3 without ice deposition and without photolysis, acquiring FTIR and mass spectra to check for contamination.

The organic residue FTIR spectrum of Exp#1 is dominated by HMT peaks (at 1461, 1366, 1235, 1045, 1005, 812 and 672 cm^{-1}; respectively labeled e, f, j, m, n, p and r in Fig. 4). Two other large peaks are present, at 1669 cm^{-1} (labeled b, probably due to C=O stretching in amides or in carboxylic acids, see the Discussion section) and a peak of formate ion (HCOO$^-$) at 1594 cm^{-1} (labeled c_2). Besides these, we observed broad peaks with low intensities which could be tentatively linked to the polymethanimine polymer (PMI) at 1355, 1209, 1091 and 970 cm^{-1} (respectively labeled g, k, l and o in Fig. 4) (Vinogradoff et al., 2012). In the corresponding mass spectra, at the end of the 300 K temperature step, no peak, which could be due to gas molecules produced from the organic residue, is observed.

We obtained the same qualitative results in two other experiments (Exp#2 and Exp#3) performed with the same initial ice composition than Exp#1 to check reproducibility. The only observed variation is that the IR absorbance is weaker in Exp #2 and #3 than in Exp#1. For example, the HMT peak at 1005 cm^{-1} is ~4 times weaker. This is probably due variations in the VUV photon fluence.
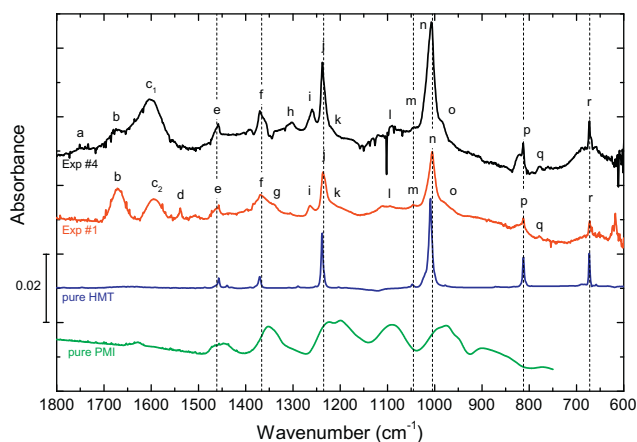
Some differences are instead observed in the FTIR spectra of the organic residue obtained in Exp#4 at 300 K, and for which CO_2 was present in the initial ice composition. HMT peaks are still the dominant features, but: (1) the peak at 1669 cm^{-1} (label b), related to a C=O stretching, has a relatively weaker absorbance than that in the FTIR spectrum of Exp#1, #2 or #3; (2) the HCOO$^-$ peak at 1594 cm^{-1} (labeled c_2 in Fig. 4) is replaced by a larger peak centered at 1601 cm^{-1} (labeled c_1 in Fig. 4), that we interpret as indicative of the presence of carboxylic acid salts (R—COO$^-$) different from the formate ion; (3) a small, broad peak is observed at

1743 cm^{-1} (labeled a in Fig. 4), which could be due to C=O stretching in esters; (4) an unidentified peak at 1302 cm^{-1} (labeled h in Fig. 4), present in FTIR spectrum of Exp#4 is absent in the spectra of Exp#1, #2 and #3.

The organic residue obtained at T = 300 K is indeed very complex, as shown by the abundance and complexity of peaks in the FTIR spectra (Fig. 4). Focusing on HMT thermal evolution, we did not investigate possible identification for all these peaks, but our results are very similar to those obtained in previous works (Bernstein et al., 1995; Muñoz Caro and Schutte, 2003), which make us confident about our experimental protocol. An exhaustive analysis of the spectra will be presented elsewhere. In the next sections, we will describe separately the time evolution of the solid and gaseous phase in Exp#1 and then in Exp#4.

4.3. Thermal evolution of experiments #1, #2 and #3 ($H_2O:CH_3OH:NH_3$ = 10:1:1)

As for the infrared spectrum at 300 K, we observe very similar thermal evolutions during Exp#1, #2 and #3. Therefore, we will only present the results of Exp#1 for which we obtained the largest production of organic material. The FTIR spectra collected at the end of each temperature step as the temperature is increased from 300 to 500 K are shown in Fig. 5. Fig. 6a show the temporal evolution of the HMT column density in the solid organic residue mea-

Table 2
Summary of organic residue peaks in FTIR spectra at 300 K.

Label	Position (cm^{-1})	Assignment	Species	References
a	1743	ν(C=O)	Esters	1, 2
b	1669	ν(C=O)	Amides, RCOOH	1
c_1	1601	ν(COO$^-$)	R–COO$^-$	
c_2	1594	ν(COO$^-$)	HCOO$^-$	3
d	1538	–	Unknown	
e	1461	δ(CH,NH)	HMT	1, 2
f	1366	δ(C–H)	HMT	1, 2
g	1355	δ(C–H)	PMI	4, 5
h	1302	–	Unknown	
i	1261		Unknown	
j	1235	ν(C–N)	HMT	1, 2
k	1209	ν(C–N)	PMI	4, 5
l	1091	ν(C–N)	PMI	4, 5
m	1045	Comb.	HMT	7
n	1005	ν(C–N)	HMT	1, 2
o	970	ν(C–N)	PMI	4, 5
p	812	ω(NH)	HMT	1, 2
q	769	δ(C–O)	HCOO$^-$	6
r	672	CNC def.	HMT	1, 2

Vibration mode: ν = stretching, δ = bending, ω = inversion, def. = deformation. Comb. = combination mode.

References. (1) Bernstein et al. (1995). (2) Muñoz Caro and Schutte (2003). (3) Vinogradoff et al. (2011). (4) Danger et al., (2011). (5) Vinogradoff et al. (2012). (6) Schutte and Buijs (1964). (7) Bertie and Solinas (1974).

Fig. 4. FTIR spectra of organic residues at 300 K for Exp#1 and Exp#4. Labels refer to peak assignments reported in Table 2. FTIR spectra of pure HMT and PMI are reported for comparison. Vertical dotted lines show the positions of the HMT peaks.

sured from FTIR spectra. To obtain the HMT column density from the 1005 and 1235 cm^{-1} peak (label n and j respectively in Fig. 4 and Table 2) we integrated their intensities over the regions reported in Bernstein et al. (1995): 1000–1020 cm^{-1} and 1228–1246 cm^{-1}, respectively, fitting the local baseline with a third order polynomial. Also, we used the integrated cross sections (A-values) reported in that same work: 5×10^{-18} cm molecule^{-1} for the peak at 1005 cm^{-1} and 2.6×10^{-18} cm molecule^{-1} for the peak at 1235 cm^{-1}.
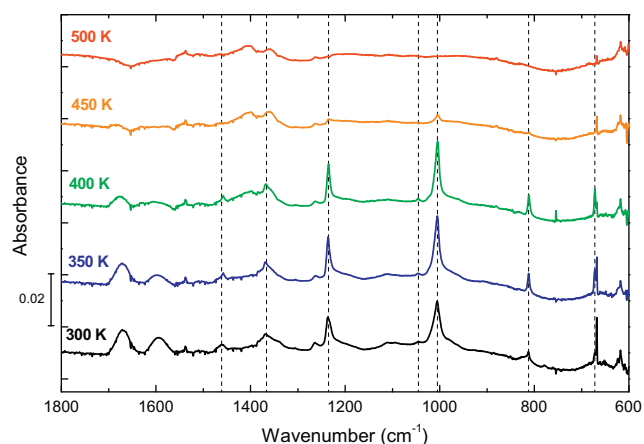
The detection of gaseous HMT in mass spectra is proved by the presence of the molecular ion peak at m/z = 140, and by the fragment peaks at m/z = 42, 56, 69, 71, 83, 85, 96, 111 and 112 (Fig. 7). This is consistent with previous measurements by Bernstein et al. (1995). Fig. 6b shows the time evolution of the intensity of the HMT molecular ion peak at m/z = 140.

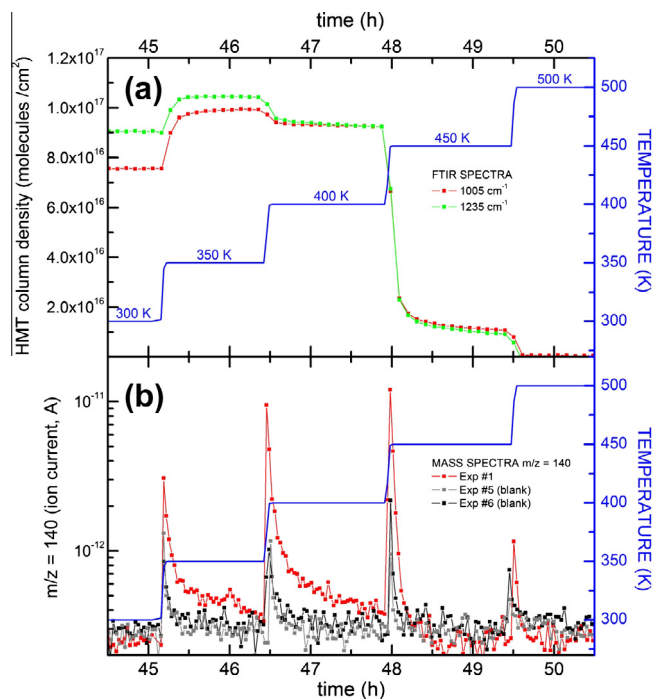### 4.3.1. First temperature step: 300 – 350 K

Increasing the temperature of the sample up to 350 K, we observe an increase of the HMT peaks in FTIR spectra (Fig. 5). This increase is fast and it seems that HMT rapidly reaches a stationary state (Fig. 6a). On the opposite, the 1594 cm^{-1} peak of formate ion and, to a lesser extent, that of C=O stretching in amides at 1669 cm^{-1}, decrease. For the gas phase, we observe that in mass spectra the HMT peak at m/z = 140 (Fig. 6b) rapidly increases and subsequently decreases. These results show that in the passage from $T = 300$ K to $T = 350$ K the amount of HMT increases in both the solid and the gas phase. When a constant temperature of 350 K is reached, the molecular ion peak at m/z = 140 does not decrease to the same intensity measured at the end of the 300 K step. Thus, it seems that a small amount of gaseous HMT is released from the solid residue while the column density of solid HMT seems to be in a stationary state.

### 4.3.2. Second temperature step: 350–400 K

Little decreases of the HMT and formate ion peaks in the FTIR spectra are observed when the temperature increases from 350 to 400 K (Fig. 5), indicating a slight decrease of the amount of these species in the solid phase. Mass spectra show again that the HMT peak at m/z = 140 clearly steps up when temperature is increased to 400 K (Fig. 6b). In particular, the HMT molecular ion peak shows an intensity one order of magnitude higher than the blank level. Its intensity rapidly decreases, but, as for the previous step, does not reach the level observed at the end of the 300 K step. Thus, produc-

Fig. 6. High temperature evolution of HMT in Exp#1. Panel (a) shows the time evolution of the column density of HMT in the solid organic residue from the FTIR peaks at 1005 cm^{-1} and 1235 cm^{-1}. Panels (b) shows the time evolution of the intensity of the mass spectrum peak at m/z = 140. The time scale is the same as in Fig. 3.
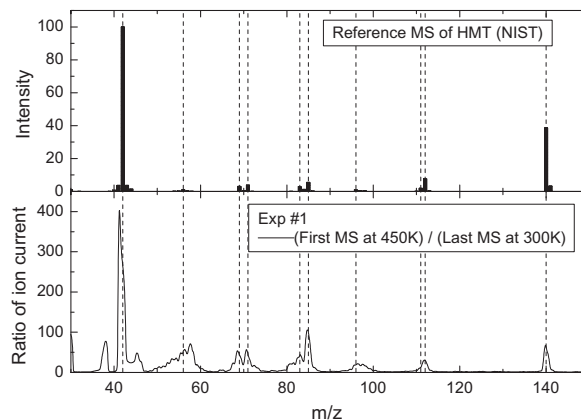
Fig. 7. Ratio of the first mass spectrum at 450 K to the last mass spectrum at 300 K acquired during Exp#1 compared to the reference mass spectrum of HMT from the NIST Chemistry Database (http://webbook.nist.gov/chemistry/). Vertical dashed lines show the position of the HMT fragment peaks at m/z = 42, 56, 69, 71, 83, 85, 96, 111, 112 and 140.

tion of gaseous HMT mainly happens in the time interval corresponding to the temperature change but seems to continue very slowly during the constant temperature time interval.

4.3.3. Third temperature step: 400–450 K

In the FTIR spectrum at 450 K the only HMT peak still visible is the one at 1005 cm^{-1} (Fig. 5) attesting of the quasi disappearance of HMT from the solid phase. Such a decrease is evident in Fig. 6a, and it appears to be very rapid: ~1 order of magnitude in ~10 min. Fig. 6a shows that 90% of the HMT is removed from the solid phase in the passage 400–450 K. When the temperature is increased to 450 K, in mass spectra the HMT peak at m/z = 140 reaches higher

Fig. 5. Evolution of the organic residue FTIR spectrum with increasing temperature for Exp#1. We report here the last FTIR spectrum acquired for each constant temperature time interval. Spectra are vertically shifted for clarity. Vertical dashed lines show the position of the HMT peaks.

intensity than in the previous temperature steps (Fig. 6b) and then it rapidly decreases to a very low level corresponding to the absence of HMT in gas phase.

4.3.4. Fourth temperature step: 450–500 K

Increasing the temperature to 500 K completely erases HMT signatures from FTIR spectra (Fig. 5). No significant HMT peaks are observed in the mass spectra at 500 K.

4.4. Thermal evolution of Exp#4 ($H_2O:CH_3OH:NH_3:CO_2$ = 10:1:1:2)

The FTIR spectra collected at the end of each temperature step of Exp#4 are shown in Fig. 8. In Fig. 9, we present the time evolution of the HMT column density in the solid organic residue measured from FTIR spectra as well as the evolution of the intensity of the HMT molecular ion peak (m/z = 140) in mass spectra, which is related to the amount of gaseous HMT.

4.4.1. First temperature step: 300–350 K

HMT peaks in the 350 K FTIR spectrum are less intense than those in the 300 K spectrum (Fig. 8). However, Fig. 9a shows that the HMT amount in the solid phase first increases when the temperature changes from 300 K to 350 K. Such an increase is limited to a few minutes, and then the HMT amount in the solid phase slowly decreases during the whole duration of the temperature step. One can note that during this temperature step, the intensity of the carboxylic acid ion band at 1601 cm^{-1} decreases. In the mass spectra, the passage 300–350 K corresponds to a strong increase of the intensity of the peak at m/z = 140 (Fig. 9b). For the whole time interval at T = 350 K, the signal of this mass spectral peak slowly decreases but remains well above the blank level. This is drastically different from what was observed in Exp#1.

4.4.2. Second temperature step: 350–400 K

Increasing the temperature to 400 K causes a strong diminution of HMT peaks in the FTIR spectrum (Fig. 8). As shown in Fig. 9a this decrease is quite slow and lasts for the whole time interval. One can note that the band at 1601 cm^{-1} does not vanish. As for the previous temperature step, the HMT amount in the gas phase increases rapidly and then the HMT molecular ion peak decreases almost to the level observed at the end of the 300 K temperature step (Fig. 9b).
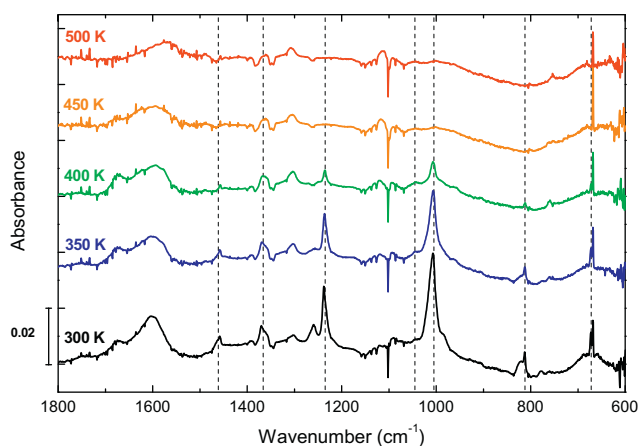
Fig. 8. Evolution of the organic residue FTIR spectrum with increasing temperature for Exp#4. We report here the last FTIR spectrum acquired for each constant temperature time interval. Spectra are vertically shifted for clarity. Vertical dashed lines show the position of the HMT peaks. The positive peak at 668 cm^{-1} is due to instability of the gaseous CO_2 in the spectrometer and the negative peak at about 1100 cm^{-1} is due to vibration generated by the cryothermostat.
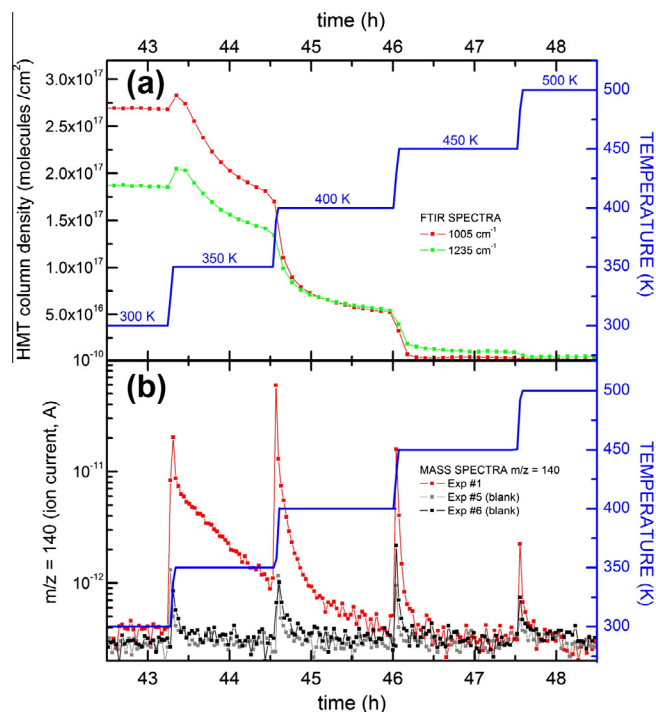
Fig. 9. High temperature evolution of HMT in Exp#4. Panel (a) shows the time evolution of the HMT column density in the solid organic residue from the FTIR peaks at 1005 cm^{-1} and 1235 cm^{-1}. Panels (b) shows the time evolution of the intensity of the mass spectrum peak at m/z = 140. The time scale is the same as that reported in Fig. 3.

4.4.3. Third temperature step: 400–450 K

No HMT peak is present in the FTIR spectrum at 450 K (Fig. 8), and therefore all the HMT has been removed from the solid phase at the end of the time interval at 450 K, contrary to what is observed in Exp#1 (Fig. 5). The evolution of FTIR spectra (Fig. 9a) reveals that HMT is rapidly removed from the solid phase when the temperature is increased to 450 K. Simultaneously, we observe a spike in the mass spectra peak at m/z = 140 (Fig. 9b) indicating release of HMT in the gas phase. The absence of significant features in both FTIR and mass spectra corresponding to the temperature step 450–500 K confirms the complete removal of HMT from our organic residue at 450 K.
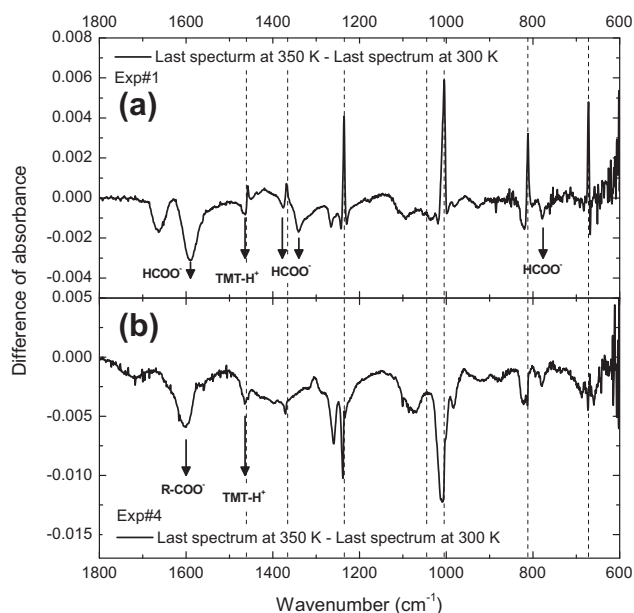
4.5. Discussion

In the organic residues synthesized by our experiments the presence of HMT at T = 300 K is firmly established by the observation of several characteristic peaks in the FTIR spectra (Fig. 4). Vinogradoff et al. (2013) described the chemical processes that take place at T < 300 K and explain the formation of HMT in our experiments. They reported that HMT forms at T > 280 K from the protonated ion of trimethylenetriamine (TMTH$^+$, $C_3H_{10}N_3^+$) and its decomposition products. A detailed chemical mechanism can be found in (Vinogradoff et al., 2012) but the last steps of HMT formation can be written:

$$2(TMTH^+; HCOO^-) \rightarrow HMT + 2\ HCOOH + 2\ NH_3 \qquad (1)$$

Fig. 10 shows the difference between the FTIR spectra of the organic residue for T = 350 K and T = 300 K. In this figure, upward peaks indicate an increase of the corresponding molecule, while downward peaks indicate a decrease. For Exp#1 (Fig. 10a) it is evident that at the end of the time interval at T = 350 K the amount of HMT in the solid phase is greater than that at T = 300 K. A more ordered crystalline structure of the solid leads to narrower and more intense absorption bands. This effect might, at least partially,

contribute to the observed changes in the HMT bands when warming from 300 to 350 K. However, Fig. 10 also shows that the amount of HCOO⁻ and TMTH⁺ decreases. The decreases of HCOO⁻ and TMTH⁺ are identified following 4 downward peaks for HCOO⁻ (Schutte et al., 1999) and one peak (1460 cm⁻¹) for TMTH⁺ (Vinogradoff et al., 2012). This indicates that the synthesis of HMT from TMTH⁺, identified by (Vinogradoff et al., 2013) for $T < 300$ K, is still active until at least 350 K. For Exp#4, Fig. 10b shows that at the end of the time interval at $T = 350$ K the amount of HMT in the solid phase is lower than that at $T = 300$ K (as observed in Fig. 9a). Fig. 10 allows highlighting some differences between the organic residue of Exp#1 and Exp#4. In particular, the different position and shape of the peak around 1600 cm⁻¹ (as observed in the FTIR spectrum at $T = 300$ K, Fig. 4) attest that the acid component of the organic residue is different in Exp#1 and Exp#4. Moreover, the comparison of panels a and b of Fig. 10 show that the behavior of HMT is drastically different in the two experiments. Nevertheless, we have to keep in mind that, for Exp#4, HMT production in the solid phase is active during the heating from 300 to 350 K (Fig. 9a) even if at the end of the 350 K step the column density of solid HMT is lower than at 300 K.

In Exp#1, the HMT absorption peaks in FTIR spectra vary significantly when the temperature increases by 50 K steps (Fig. 6a) but we observed little variations during the time intervals at constant temperature. This suggests that the chemistry inside the solid organic residue rapidly goes toward a quasi-stationary state after each temperature increment. In contrast, in Exp#4 we observe significant variations of the FTIR spectra during the time intervals at constant temperature (Fig. 9a): increasing the temperature from 300 K to 350 K induces an increase of HMT in the organic residue, but then, at $T = 350$ K, the amount of HMT clearly decreases and such a decrease continues during the whole time interval at $T = 400$ K. Thus, the kinetics of the thermal evolution is different between Exp#1 and Exp#4 (Fig. 10). We interpret these differences as being due to the different molecular composition of the organic

residues at $T = 300$ K in the two experiments (Fig. 4), which results from the different initial ice composition (we added CO₂ for Exp#4). This shows that the molecular composition of the initial ice mixture determine not only the composition of the organic residue at $T = 300$ K (Fig. 4), but also the kinetics of its thermal evolution above this temperature. The comparison of Figs. 6a and 9a, as well as Fig. 10, show that the evolution of a given molecule (HMT) strongly depends on the nature of the organic compound that surrounds this molecule.

Concerning the gas phase sampled by mass spectrometry, the effect of the 50 K temperature steps is a very rapid increase of the peak intensity. The observation of the molecular ion peak at m/z = 140 and of the fragment peaks (Fig. 7) attests that HMT is also present in gas phase. In particular, the intensity of the HMT peaks at m/z = 140 (molecular ion) is clearly above the blank level when the temperature is increased (Figs. 6b and 9b). Then, at constant temperature, we observe that HMT peaks gradually decrease with a kinetic that depends of the molecular composition of the organic residue in which the HMT is embedded. In addition, the evolution of mass spectra with increasing temperature is correlated with that of HMT FTIR spectra: the temperature steps, for which the signal of gaseous HMT is the highest in both Exp#1 and Exp#4, are those for which the loss of solid HMT is the most important. This shows that gaseous HMT is produced by sublimation during the rapid temperature increments, and that the sublimation continues at constant temperature, gradually fading down.

The sublimation curve $P(T)$ for pure HMT can be calculated from the Clapeyron equation:

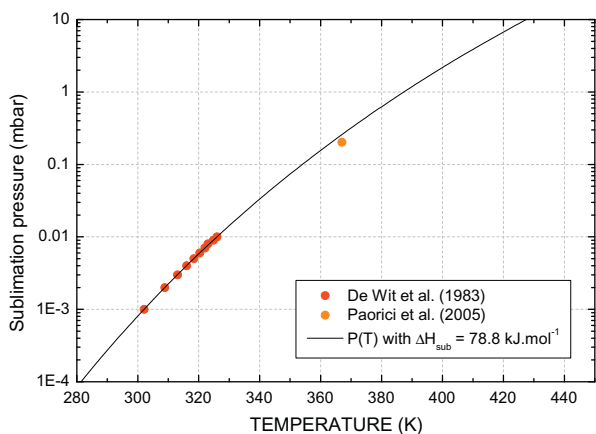$$\frac{dP}{dT} = \frac{\Delta H_S(T)}{T \Delta V} \tag{2}$$

where P is the pressure (in Pa), T the temperature (in K), ΔH_S the enthalpy of sublimation (in J/mol), and ΔV is the variation of molar volume (in m³/mol). In the case of HMT, the gas molar volume V_{gas} is larger than the solid molar volume V_{solid} by several orders of magnitude. As the HMT sublimation pressure is quite low (see below) we can use the perfect gas hypothesis. In such case, we have $\Delta V = V_{gas} - V_{solid} \approx V_{gas} = RT/P$ ($R = 8.314$ J/mol/K). Moreover, if we suppose $\Delta H_S(T) \approx$ constant, the relation for the sublimation curve $P(T)$ is:

$$\ln\left(\frac{P}{P_0}\right) \approx \frac{\Delta H_S}{R}\left(\frac{1}{T_0} - \frac{1}{T}\right) \tag{3}$$

Using the thermodynamic data reported in (De Wit et al., 1983) ($\Delta H_S = 78.8$ kJ/mol and $P_0(T_0 = 316$ K) = 0.4 Pa), the sublimation pressure of pure HMT in the 280–450 K temperature range can be calculated (Fig. 11). We note that our extrapolation reproduces quite well the sublimation pressure of pure HMT independently measured at 367 K (Paorici et al., 2005).

At 300 K, the vapor pressure of pure HMT is about 10⁻³ mbar. At the end of the 300 K time interval (16 h), we observed no gaseous HMT (Figs. 6b and 9b). Solid HMT is present in the organic residue at 300 K whereas the pressure in the vacuum chamber is lower than the sublimation pressure of pure HMT by several orders of magnitude, as previously reported (Bernstein et al., 1995; Muñoz Caro et al., 2004). This shows: (1) that the kinetics of HMT sublimation is greatly changed by the fact that HMT is part of the organic residue matrix; and (2) that the interactions between HMT and others molecules of the organic residue, via hydrogen bonds or Van der Waals forces, are quite strong and prevent the HMT sublimation. The comparison between the behavior of HMT as pure compound and embedded in an organic matrix show that the sublimation or thermal desorption of HMT depends of its environment.

We observe that HMT production in the solid phase and HMT sublimation are simultaneous processes when the temperature

Fig. 10. Difference between the organic residue FTIR spectra measured at $T = 350$ K and at $T = 300$ K during Exp#1 (a) and Exp#4 (b). Upward peaks indicate an increase of the corresponding molecule, while downward peaks indicate a decrease. Vertical dashed lines show the position of the HMT peaks. (a) In Exp#1 the amount of HMT increases, while those of HCOO⁻ and TMTH⁺ decrease, confirming reaction (1). The presence of other upward and downward peaks shows that this is not the only process caused by heating. (b) In Exp#4 the amount of HMT decreases.

Fig. 11. pure HMT sublimation curve (see text for details). Dots are the values measured by De Wit et al. (1983) and Paorici et al. (2005). The value of sublimation enthalpy (ΔH_S = 78.8 kJ/mol) comes from De Wit et al. (1983).

increases above 300 K. The most obvious case is the 300–350 K temperature increment in Exp#1, during which we observe an increase of both solid and gaseous HMT (Fig 6a and b). In order to roughly estimate the intensity of both processes we can compare the integral of the mass peak at m/z = 140 over the time of each temperature step with the variation of the column density observed from infrared spectra. For Exp#1, the integral of the m/z = 140 mass peak is about 2.2×10^{-9} A s, 4.9×10^{-9} A s and 3.6×10^{-9} A s for the 350, 400, and 450 K time intervals, respectively (see Fig. 6b). During the same time intervals, considering that the surface of the sample holder is about 1 cm^2, we observed that the variations of the number of HMT molecules are about $+2 \times 10^{16}$ molecules, -0.7×10^{16} molecules and -8.2×10^{16} molecules (see Fig. 6a). Careful examination of the last infrared spectra measured at 400 K and 450 K show that there is no more HMT production during the 400–450 K temperature step, contrary to the previous ones. We can therefore estimate that for the m/z = 140 peak an integrated signal of 3.6×10^{-9} A s correspond to the sublimation of about 8.2×10^{16} molecules. Thus, we can estimate that during the 350 K and 400 K temperature time intervals, about 5×10^{16} and 11×10^{16} HMT molecules, respectively, sublimate. Thus, during the 350 K temperature step, we have a production of about 7×10^{16} molecules of HMT. About 30% of this production is remaining in the solid phase while 70% sublimates. Similarly, during the 400 K temperature step, the decrease of solid HMT is about 0.7×10^{16} molecules and sublimation represents 11×10^{16} molecules, thus the production of HMT should be at least of 10×10^{16} molecules. All these numbers have to be considered as orders of magnitude; nevertheless they show that the sublimation is a very efficient process and that most of the HMT produced in the solid phase sublimates immediately. This conclusion is coherent with the fact that the sublimation pressure of pure HMT is several orders of magnitude higher than the pressure in the experimental setup at these temperatures. Moreover the production during the 350 K and 400 K temperature steps is of the same order than the production which has taken place for temperature below 300 K. It means that the precursors of HMT could be more abundant in the residue at 300 K than the HMT itself. Similar conclusion could be drawn from Exp#4, whereas in this second case it is possible that the production of HMT is still occurring during the 400–450 K increment.

The quantitative description of the kinetics of the thermal evolution of HMT in organic residues is important as it could be used to extrapolated laboratory results to astrophysical environment. Unfortunately, the complete description of the kinetics seems to

be very complex as different mechanism of formation and sublimation take place simultaneously and as HMT sublimation clearly depends of the molecular environment via different interactions with the organic matrix in which it is embedded.

The peak at 1669 cm^{-1} is a major feature in the organic residue FTIR spectra at 300 K (Fig. 4). We note that this peak appears at the same time than the HMT ones for temperatures comprised between 260 and 300 K (see Fig. 7 of Vinogradoff et al. (2013)). Thus, it is linked to a product of a chemical reaction promoted by the temperature increase and cannot be attributed to a product of the initial VUV photolysis. The molecular attribution of this peak is quite difficult, but it could be identified as a C=O stretching. Bernstein et al. (1995) observed a peak at 1665 cm^{-1} in the organic residue synthesized from VUV photolysis and warming of a H$_2$O:NH$_3$:CH$_3$OH:CO = 100:10:50:10 ice mixture. The authors assigned it to C=O stretching in primary amides (H$_2$N=C(=O)=R). Muñoz Caro and Schutte (2003) observed a peak at 1680 cm^{-1} in the organic residue synthesized in a similar way, and they also assigned it to C=O stretching in amides. The precise molecular attribution of such feature in FTIR spectra is beyond the scopes of this work. However we qualitatively observe that it decreases with increasing temperature. In Exp#1 (Fig. 5) and Exp#4 (Fig. 8) its decrease is particularly evident when the temperature increases from 400 K to 450 K, when at the same time HMT is totally removed from the solid phase.

5. Implications for the search of HMT in comets

Our laboratory simulations indicate that HMT can be trapped up to 450 K in the solid organic residue produced by VUV photolysis of an H$_2$O, CH$_3$OH, NH$_3$ ice mixture, and up to 400 K when CO$_2$ is added to the initial ice composition. Vinogradoff et al. (2013), which studied the low temperature (T < 300 K) evolution of the same organic residue (same as Exp#1), reported that HMT is formed in the solid phase only when the temperature reaches >280 K in laboratory conditions. Theoretical calculations have shown that the last step of the HMT formation has an action barrier of 90 kJ mol^{-1} (Vinogradoff et al., 2012). The formation of HMT could take place at lower temperature but on large time scales. Preliminary kinetic results showed that the HMT formation would require ~5×10^4 years at 200 K (Vinogradoff et al., 2013). These observations have crucial implications on the possible astrophysical contexts in which HMT may be present in the solid phase. HMT could not have been formed in materials that have always experienced very low temperature, and in materials heated at high temperature (T > 450 K) HMT would not be present because it sublimates. Consequently, HMT can be present in materials only which have been slightly heated, between 280 K and 400 K. Temperatures suitable for HMT formation were certainly reached in the nascent Solar System. Since comets accreted materials from both the outer, cold Solar System regions and the inner, warm regions, then cometary nuclei could contain a small fraction of HMT.

In this context, the upcoming cometary mission Rosetta is of primary importance, as it will perform *in situ* analyses of the nucleus and the environment of Comet 67P/Churyumov–Gerasimenko, starting in 2014. If HMT was detected by the Rosetta mission in solid organic material of Comet 67P/Churyumov–Gerasimenko, it would be a very strong indicator of its thermal history. Temperatures suitable for HMT formation were determined at the surface of the nucleus of Comet 1P/Halley (320 K as mean value, 400 K as maximum value, (Emerich et al., 1987), and the nucleus of Comet 19P/Borrelly (300–340 K, (Soderblom et al., 2004). However, similar temperatures can be experienced by dust grains ejected from the nucleus (Fray et al., 2006). Therefore HMT could form directly from refractory organics in the cometary coma. On

board Rosetta, the most promising instrument for the detection of organic species in solid phase is COSIMA (Kissel et al., 2007). COSIMA is a high mass resolution, time-of-flight secondary ion mass spectrometer (TOF-SIMS) designed for the collection and the analysis of cometary grains in the coma. Preliminary calibration experiments performed with the ground model of COSIMA on organic residues similar to the ones presented in this paper show that the HMT signature is highly specific and then detectable by COSIMA.

As we showed that HMT sublimation is an important process, the Rosetta mission should also search for HMT in the gas phase. We have to keep in mind that HMT cannot be detected at sub-millimetric wavelengths by remote sensing measurements, because it belongs to the Td symmetry group (Jensen, 2002) and thus has no permanent dipole and no allowed rotational transition. Some attempts could be performed in the infrared range. Among the Rosetta instruments, the VIRTIS infrared spectrometer will investigate the coma gaseous species in the 1–5 μm wavelength range (Coradini et al., 2007). Nevertheless, the most sensitive Rosetta instrument for searching for HMT in the gas phase will be ROSINA, which consists in two mass spectrometers, one for neutrals species and the other one for primary ions (Balsiger et al., 2007). Moreover, it has also already been shown that COSAC, which is a gas chromatograph coupled to a mass spectrometer on board of the Rosetta lander, has the capability to detect HMT directly at the surface of the nucleus (Cottin et al., 2001).

Therefore, the Rosetta space mission will have the ability to search for direct evidence of cometary HMT in both solid and gaseous phases, using the COSIMA and ROSINA spectrometers, respectively. This simultaneous search will be of crucial importance to have an unambiguous detection of HMT. Indeed, as cometary grains collected by the COSIMA time-of-flight spectrometer will experience temperatures between 253 K and 303 K during several days before analysis (Kissel et al., 2007), HMT could form inside the instrument. Therefore, the ROSINA measurements will be essential to have confirmation of any possible detection of HMT in the cometary solid phase by COSIMA.

6. Conclusions

We experimentally simulated the thermal evolution of refractory organic residues synthesized by photolysis and subsequent warming of astrophysical ice analogues. We investigated the thermal evolution of the refractory organic material heated up to 550 K. We focused our attention on HMT, a molecule often produced in this kind of experimental simulations but never observed in the interstellar medium or in comets, so far.

In laboratory conditions, HMT is formed in the solid organic residue from the protonated ion of trimethylenetriamine (TMTH$^+$) and its decomposition products at $T > 280$ K (Vinogradoff et al., 2013). We were able to show that such a process is still active at temperatures as high as 350 K. For temperature higher than 300 K the HMT amount inside the solid organic residue is reduced by sublimation, rather than by decomposition to other molecules. Solid HMT production and sublimation take place simultaneously and the amount of HMT observed in the solid phase can be only a minor fraction of the total production of HMT, as a major fraction of HMT could disappear from the organic residue by sublimation. The quantitative measurements of the kinetics of each process seem to be very complex.

An important parameter that drives the HMT thermal evolution is the molecular composition of the organic residue in which it is embedded. Depending on the composition of the residue, HMT could be present in solid phase up to 400 or 450 K. Therefore, in

an astrophysical environment, HMT can be present in the solid phase only in a very narrow temperature range (280 K < T < 400 K).

The upcoming space mission Rosetta, which will study Comet 67P/Churyumov–Gerasimenko for several months during its approach to the Sun, will investigate if HMT is present in this comet. Solid cometary grains ejected from the nucleus will be analyzed by the COSIMA time-of-flight mass spectrometer. At the same time, the ROSINA spectrometer will analyze the gas species in the coma. Thus, the Rosetta mission has the capacities to detect HMT in both the solid and gaseous phase. A detection of HMT will provide important indications on the thermal history of the cometary grains.

References

Balsiger, H. et al., 2007. Rosina – Rosetta orbiter spectrometer for ion and neutral analysis. Space Sci. Rev. 128, 745–801.

Bernstein, M.P., Sandford, S.A., Allamandola, L.J., Chang, S., Scharberg, M.A., 1995. Organic compounds produced by photolysis of realistic interstellar and cometary ice analogs containing methanol. Astrophys. J. 454, 327–344.

Bertie, J.E., Solinas, M., 1974. Infrared and Raman spectra and the vibrational assignment of hexamethylenetetramine-h$_{12}$ and -d$_{12}$. J. Chem. Phys. 61, 1666–1677.

Bockelée-Morvan, D., Crovisier, J., Mumma, M.J., Weaver, H.A., 2004. The composition of cometary volatiles. In: Festou, M.C., Keller, H.U., Weaver, H.A. (Eds.), Comets II. The University of Arizona Press, pp. 391–423.

Bossa, J.B., Duvernay, F., Theule, P., Borget, F., d'Hendecourt, L., Chiavassa, T., 2009. Methylammonium methylcarbamate thermal formation in interstellar ice analogs: A glycine salt precursor in protostellar environments. Astron. Astrophys. 506, 601–608.

Bradley, J.P., 2003. Interplanery dust particles. In: Davis, A.M., Holland, H.D., Turekian, K.K. (Eds.), Treatise on Geochemistry, vol. 1. Elsevier, pp. 689–711.

Brownlee, D.E., 2003. Comets. In: Davis, A.M., Holland, H.D., Turekian, K.K. (Eds.). Treatise on Geochemistry, vol. 1. Elsevier, pp. 663–688.

Chyba, C.F., Thomas, P.J., Brookshaw, L., Sagan, C., 1990. Cometary delivery of organic molecules to the early Earth. Science 249, 366–373.

Clemett, S.J., Maechling, C.R., Zare, R.N., Swan, P.D., Walker, R.M., 1993. Identification of complex aromatic molecules in individual interplanetary dust particles. Science 262, 721–725.

Colangeli, L., Brucato, J.R., Bar-Nun, A., Hudson, R.L. Moore, M.H., 2004, Laboratory experiments on cometary materials. In: Festou, M.C., Keller, H.U., Weaver, H.A. (Eds.), Comets II. The University of Arizona Press, pp. 695–717.

Coradini, A. et al., 2007. Virtis: An imaging spectrometer for the Rosetta Mission. Space Sci. Rev. 128, 529–559.

Cottin, H., Fray, N., 2008. Distributed sources in Comets. Space Sci. Rev. 138, 179–197.

Cottin, H., Gazeau, M.C., Raulin, F., 1999. Cometary organic chemistry: A review from observations, numerical and experimental simulations. Planet. Space Sci. 47, 1141–1162.

Cottin, H., Szopa, C., Moore, M.H., 2001. Production of hexamethylenetetramine in photolyzed and irradiated interstellar cometary ice analogs. Astrophys. J. 561, L139–L142.

Crovisier, J. et al., 1997. The spectrum of Comet Hale–Bopp (C/1995 01) observed with the Infrared Space Observatory at 2.9 AU from the Sun. Science 275, 1904–1907.

Crovisier, J. et al., 2000. The Thermal Infrared Spectra of Comets Hale–Bopp and 103P/Hartley 2 Observed with the Infrared Space Observatory. Thermal Emiss. Spectrosc. Anal. Dust, Disks, Regoliths 196, 109–117.

Danger, G., Borget, F., Chomat, M., Duvernay, F., Theulé, P., Guillemin, J.-C., Le Sergeant D'Hendecourt, L., Chiavassa, T., 2011. Experimental investigation of aminoacetonitrile formation through the Strecker synthesis in astrophysical-like conditions: reactivity of methanimine (CH$_2$NH), ammonia (NH$_3$), and hydrogen cyanide (HCN). Astron. Astrophys. 535, A47–A54.

Dartois, E., 2005. The Ice Survey Opportunity of ISO. Space Sci. Rev. 119, 293–310.

Davidson, J., Busemann, H., Franchi, I.A., 2012. A NanoSIMS and Raman spectroscopic comparison of interplanetary dust particles from Comet Grigg–Skjellerup and non-Grigg Skjellerup collections. Meteorit. Planet. Sci. 47, 1748–1771.

Davis, D., Braun, W., 1968. Intense vacuum ultraviolet atomic line sources. Appl. Opt. 7, 2071–2074.

De Wit, H.G.M., Van Miltenburg, J.C., De Kruif, C.G., 1983. Thermodynamic properties of molecular organic crystals containing nitrogen, oxygen, and sulphur 1. vapour pressures and enthalpies of sublimation. J. Chem. Thermodynam. 15, 651–663.

Dobrică, E., Engrand, C., Quirico, E., Montagnac, G., Duprat, J., 2011. Raman characterization of carbonaceous matter in CONCORDIA Antarctic micrometeorites. Meteorit. Planet. Sci. 46, 1363–1375.

Duprat, J. et al., 2010. Extreme deuterium excesses in ultracarbonaceous micrometeorites from central Antarctic snow. Science 328, 742–745.

Elsila, J.E., Glavin, D.P., Dworkin, J.P., 2009. Cometary glycine detected in samples returned by Stardust. Meteorit. Planet. Sci. 44, 1323–1330.

Emerich, C. et al., 1987. Temperature and size of the nucleus of Comet p/Halley deduced from IKS infrared VEGA-1 measurements. Astron. Astrophys. 187, 839–842.

Floss, C. et al., 2006. Identification of isotopically primitive interplanetary dust particles: A NanoSIMS isotopic imaging study. Geochim. Cosmochim. Acta 70, 2371–2399.

Flynn, G.J., 2008. Physical, chemical, and mineralogical properties of Comet 81P/Wild 2 particles collected by Stardust. Earth Moon Planets 102, 447–459.

Flynn, G., Keller, L.P., Jacobsen, C., Wirick, S., Miller, M.A., 2000. Organic carbon in interplanetary dust particles. In: Lemarchand, G., Meech, K. (Eds.), Bioastronomy '99: a new era in bioastronomy. Astronomical Society of the Pacific, vol 213, pp. 191–194.

Fomenkova, M.N., 1999. On the organic refractory component of cometary dust. Space Sci. Rev. 90, 109–114.

Fomenkova, M.N., Chang, S., Mukhin, L.M., 1994. Carbonaceous components in the Comet Halley dust. Geochim. Cosmochim. Acta 58, 4503–4512.

Fray, N., Bénilan, Y., Cottin, H. & Gazeau, M.-C. (2004), New experimental results on the degradation of polyoxymethylene: Application to the origin of the formaldehyde extended source in comets, J. Geophys. Res. (Planets) 109, E07S12, 1–7.

Fray, N., Bénilan, Y., Biver, N., Bockelée-Morvan, D., Cottin, H., Crovisier, J., Gazeau, M.-C., 2006. Heliocentric evolution of the degradation of polyoxymethylene: Application to the origin of the formaldehyde (H_2CO) extended source in Comet C/1995 O1 (Hale Bopp). Icarus 184, 239–254.

Gerakines, P.A., Schutte, W.A., Greenberg, J.M., van Dishoeck, E.F., 1995. The infrared band strengths of H_2O, CO and CO_2 in laboratory simulations of astrophysical ice mixtures. Astron. Astrophys. 296, 810–818.

Gibb, E.L., Whittet, D.C.B., Boogert, A.C.A., Tielens, A.G.G.M., 2004. Interstellar ice: The Infrared Space Observatory legacy. Astrophys. J. Suppl. Ser. 151, 35–73.

Gounelle, M., 2011. The asteroid–comet continuum: in search of lost primitivity. Elements 7, 29–34.

Greenberg, J.M., 1982. What Are Comets Made Of? A Model Based on Interstellar Dust. University of Arizona Press, pp. 131–163.

Hanner, M.S., Bradley, J.P., 2004. Composition and mineralogy of cometary dust. In: Festou, M.C., Keller, H.U., Weaver, H.A. (Eds.), Comets II. The University of Arizona Press, pp. 555–564.

Jensen, J.O., 2002. Vibrational frequencies and structural determinations of hexamethylenetetramine. Spectrochim. Acta Part A: Mol. Biomol. Spectrosc. 58, 1347–1364.

Keller, L.P. et al., 2006. Infrared spectroscopy of Comet 81P/Wild 2 samples returned by Stardust. Science 314, 1728–1731.

Kissel, J. et al., 1986a. Composition of Comet Halley dust particles from Giotto observations. Nature. 321, 336–338.

Kissel, J. et al., 1986b. Composition of Comet Halley dust particles from VEGA observations. Nature 321, 280–282.

Kissel, J., Krueger, F.R., Silén, J., Clark, B.C., 2004. The cometary and interstellar dust analyzer at Comet 81P/Wild 2. Science 304, 1774–1776.

Kissel, J. et al., 2007. Cosima high resolution time-of-flight secondary ion mass spectrometer for the analysis of cometary dust particles onboard Rosetta. Space Sci. Rev. 128, 823–867.

Kolokolova, L., Hanner, M.S., Levasseur-Regourd, A.-C., Gustafson, B.A.S., 2004. Physical properties of cometary dust from light scattering and thermal emission. In: Festou, M.C., Keller, H.U., Weaver, H.A. (Eds.), Comets II. The University of Arizona Press, pp. 577–604.

Le Roy, L. et al., 2012. On the prospective detection of polyoxymethylene in Comet 67P/Churyumov–Gerasimenko with the COSIMA instrument onboard Rosetta. Planet. Space Sci. 65, 83–92.

Lellouch, E. et al., 1998. Evidence for water ice and estimate of dust production rate in Comet Hale–Bopp at 2.9 AU from the Sun. Astron. Astrophys. 339, L9–L12.

Mason, N.J. et al., 2006. VUV spectroscopy and photo-processing of astrochemical ices: an experimental study. Faraday Discuss. 133, 311–329.

Matrajt, G., Messenger, S., Brownlee, D., Joswiak, D., 2012. Diverse forms of primordial organic matter identified in interplanetary dust particles. Meteorit. Planet. Sci. 47, 525–549.

Meinert, C., Filippi, J.-J., de Marcellus, P., Le Sergeant d'Hendecourt, L., Meierhenrich, U.J., 2012. N-(2-aminoethyl)glycine and amino acids from interstellar ice analogues. ChemPlusChem 77 (3), 186–191.

Muñoz Caro, G.M., Schutte, W.A., 2003. UV-photoprocessing of interstellar ice analogs: New infrared spectroscopic results. Astron. Astrophys. 412, 121–132.

Muñoz Caro, G.M., Meierhenrich, U., Schutte, W.A., Thiemann, W.H.-P., Greenberg, J.M., 2004. UV-photoprocessing of interstellar ice analogs: Detection of hexamethylenetetramine-based species. Astron. Astrophys. 413, 209–216.

Muñoz Caro, G.M. et al., 2006. Nature and evolution of the dominant carbonaceous matter in interplanetary dust particles: effects of irradiation and identification with a type of amorphous carbon. Astron. Astrophys. 459, 147–159.

Muñoz Caro, G.M., Dartois, E., Nakamura-Messenger, K., 2008. Characterization of the carbon component in cometary Stardust samples by means of infrared and Raman spectroscopy. Astron. Astrophys. 485, 743–751.

Paorici, C., Zha, M., Razzetti, C., Zanotti, L., Bassano, E., Castagnolo, D., 2005. Progressive growth rate reduction due to impurity desorption in vapor grown hexamethylenetetramine crystals. Cryst. Res. Technol. 40, 1076–1081.

Sandford, S.A. et al., 2006. Organics captured from Comet 81P/Wild 2 by the Stardust spacecraft. Science 314, 1720–1724.

Sandford, S.A. et al., 2010. Assessment and control of organic and other contaminants associated with the Stardust sample return from Comet 81P/Wild 2. Meteorit. Planet. Sci. 45, 406–433.

Schutte, C.J.H., Buijs, K., 1964. The infrared spectrum of the formate ion. Spectrochim. Acta 20, 187–195.

Schutte, W.A. et al., 1999. Weak ice absorption features at 7.24 and 7.41 MU M in the spectrum of the obscured young stellar object W 33A. Astron. Astrophys. 343, 966–976.

Soderblom, L.A., Britt, D.T., Brown, R.H., Buratti, B.J., Kirk, R.L., Owen, T.C., Yelle, R.V., 2004. Short-wavelength infrared (1.3–2.6 μm) observations of the nucleus of Comet 19P/Borrelly. Icarus 167, 100–112.

Sunshine, J.M. et al., 2006. Exposed water ice deposits on the surface of Comet 9P/Tempel 1. Science 311, 1453–1455.

Vinogradoff, V., Duvernay, F., Danger, G., Theulé, P., Chiavassa, T., 2011. New insight into the formation of hexamethylenetetramine (HMT) in interstellar and cometary ice analogs. Astron. Astrophys. 530, A128–A134.

Vinogradoff, V., Rimola, A., Duvernay, F., Danger, G., Theulé, P., Chiavassa, T., 2012. The mechanism of hexamethylenetetramine (HMT) formation in the solid state at low temperature. Phys. Chem. Chem. Phys. (Incorporat. Faraday Trans.) 14, 12309–12320.

Vinogradoff, V. et al., 2013. Importance of thermal reactivity for hexamethylenetetramine formation from simulated interstellar ices. Astron. Astrophys. 551, A128–A136.

Warneck, P., 1962. A microwave-powered hydrogen lamp for vacuum ultraviolet photochemical research. Appl. Opt. 1, 721–726.

Wooden, D., Desch, S., Harker, D., Gail, H.-P., Keller, L. (2007), Comet grains and implications for heating and radial mixing in the protoplanetary disk. In: Reipurth, B., Jewitt, D., Keil, K. (Eds.), Protostars and Planets V. The University of Arizona Press, pp. 815–833.

Zolensky, M.E. et al., 2006. Mineralogy and petrology of Comet 81P/Wild 2 nucleus samples. Science 314, 1735–1739.